Journal of the Korean Crystal Growth and Crystal Technology
Vol. 24, No. 3 (2014) 111-119
http://dx.doi.org/10.6111/JKCGCT.2014.24.3.111

p-ISSN 1225-1429
e-ISSN 2234-5078

Synthesis of scheelite-type nanocolloidal particles by pulsed laser ablation in liquid and their size distribution analysis

Jung-Il Lee, Kwang Bo Shim* and Jeong Ho Ryu†

Department of Materials Science and Engineering, Korea National University of Transportation, Chungju 380-702, Korea
**Division of Materials Science and Engineering, Hanyang University, Seoul 133-791, Korea*

(Received May 28, 2014)
(Revised June 9, 2014)
(Accepted June 13, 2014)

Abstract A novel pulsed laser ablation process in liquid was investigated to prepare scheelite-type ceramic [calcium tungstate ($CaWO_4$) and calcium molybdate ($CaMoO_4$)] nanocolloidal particles. The crystalline phase, particle morphology, particle size distribution, absorbance and optical band-gap were investigated. Stable colloidal suspensions consisting of well-dispersed $CaWO_4$ and $CaMoO_4$ nanoparticles with narrow size distribution could be obtained without any surfactant. Particle tracking analysis using optical microscope combined with image analysis was applied for a fast determination of particle size distribution in the prepared nanocolloidal suspensions. The mean nanoparticle size of $CaWO_4$ and $CaMoO_4$ colloidal nanoparticles were 16 nm and 30 nm, with the standard deviations of 2.1 and 5.2 nm, respectively. The optical absorption edges showed blue-shifted values about 60~70 nm than those of reported in bulk crystals. And also, the estimated optical energy band-gaps of $CaWO_4$ and $CaMoO_4$ colloidal particles were 5.2 and 4.7 eV. The observed band-gap widening and blue-shift of the optical absorbance could be ascribed to the quantum confinement effect due to the very small size of the $CaWO_4$ and $CaMoO_4$ nanocolloidal particles prepared by pulsed laser ablation in liquid.

Key words Pulsed laser ablation, Nanocolloidal suspensions, $CaWO_4$ and $CaMoO_4$, Size distribution, Particle tracking analysis, Blue-shift

1. Introduction

Pulsed laser ablation (PLA) in liquids attracts much attention as a new technique to prepare nanocolloidal particles since Henglein, Cotton and their co-workers first developed this synthesis strategy [1, 2]. It has been demonstrated that laser ablation of various noble metals settled in solvents produces colloidal nanoparticles of these metals [3-5]. A remarkable advantage of this laser ablation method over chemical synthesis is simplicity of preparation procedures. Moreover, it has shown that the laser ablation in liquids is applicable to prepare nanoparticles of not only noble metals but also compound materials. It was reported that laser ablation of TiO_2 [6], ZnSe [7], GaAs [8] and CoO [9] in various solvents produced nanoparticles of these materials. Above studies on noble metals and compound materials have shown that stoichiometric nanoparticles could be produced by using laser ablation in liquids, i.e., atomic compositions of produced nanoparticles were identical to those of their source materials.

†Corresponding author
Tel: +82-43-841-5384
Fax: +82-43-841-5380
E-mail: jhryu@ut.ac.kr

In addition, reliable and fast determination of particle size distributions in sub-micrometer ranges still poses a certain challenge for common analytical equipment. Comparative studies [10-12] revealed remarkable differences between size distribution functions derived from different techniques. Generally, the most useful approaches also tend to be the most expensive and time consuming [13]. While dynamic light scattering offers the advantage of being fast and convenient, it lacks precision when dealing with multi-modal distributions. Therefore a more sophisticated approach is represented using Brownian motion of the particles sensed by the frequency shift of scattered light. In this case, a complete paricle ensemble is analyzed collectively, leading to an autocorrelation function that is linked to the particle size distribution. Under such circumstances, an analysis of the size distribution function from the characteristics of Brownian motion requires the independent detection of a number of individual particles [14-16], leading to the assignment of individual mean square displacements and individual particle sizes. This technique is suitable for particles in the sub-micrometer range because it requires no specific sample preparation and even allows for a selective analysis of components in particle mixtures.

Calcium tungstate ($CaWO_4$, scheelite) and calcium

molybdate ($CaMoO_4$, powellite) is an important material among metal tungstate or molybdate families that have a high application potential in various fields, such as in photoluminescence and microwave applications [17, 18]. Various methods, such as Czochralski method, coprecipitation synthesis, combustion method and solid-state reaction have been used to synthesize $CaWO_4$ and/or $CaMoO_4$ [19-21]. However, $CaWO_4$ and/or $CaMoO_4$ particles prepared by these processes are relatively large with irregular morphology, and inhomogeneous compounds might be easily formed because WO_3 and MoO_3 have tendency to vaporize at high temperatures [22].

This work represents a new synthetic approach to directly produce highly-dispersed $CaWO_4$ and $CaMoO_4$ nanocolloidal suspensions using pulsed laser ablation (PLA) ceramic target in a liquid phase without any surfactant. Crystallization process, particle morphology, laser ablation mechanism and optical properties were analyzed. Moreover, a novel method is presented for the fast determination of nanoparticle size distributions, which is based on simultaneous motion tracking of several individual particles in a particle ensemble.

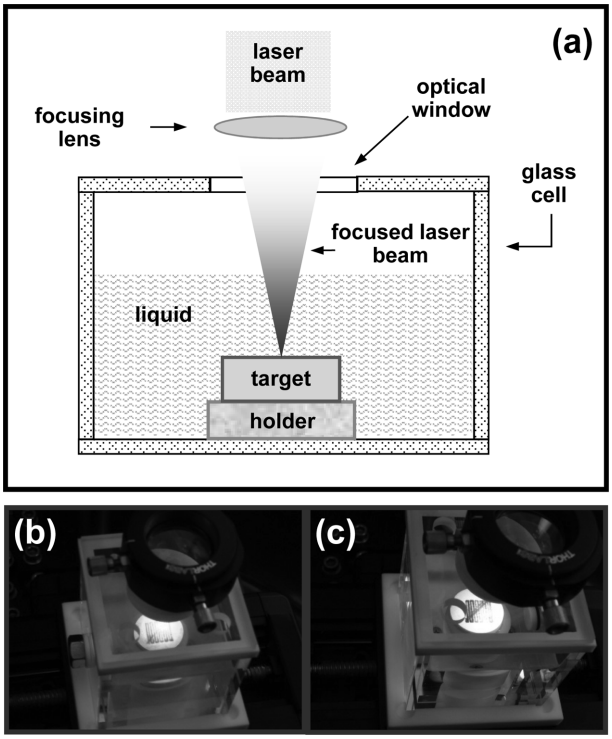

Fig. 1. Schematic diagram for the laser ablation of target in liquid phase (a) and experimental photographs of (b) $CaWO_4$ and (b) $CaMoO_4$ targets during laser ablation in ethanol.

2. Experimental

2.1. Synthesis of Nanocolloidal Suspensions by Laser Ablation in Ethanol

Laser ablation of $CaWO_4$ and $CaMoO_4$ in ethanol were carried out using a fourth harmonic (266 nm) of a Nd : YAG pulse laser (Quentel, France) with a repetition rate of 10 Hz, pulse width of 8 ns and a maximum output of 100 mJ/pulse. The laser beam strikes the surface vertically after passing throughout an optical window and the liquid. Fig. 1(a~c) shows experimental set-ups, composed of a glass cell, liquid, a ceramic target on a Teflon holder and laser beam crossing the liquid for synthesizing $CaWO_4$ and $CaMoO_4$ nanocolloidal suspensions, respectively. To avoid the formation of deep holes, the glass cell was displaced under the laser beam using a computer-driven X-Y stage with laser scanning velocity of 0.5 mm/sec and 70~80 % overlaps of the laser spot between the consecutive scans.

The $CaWO_4$ and $CaMoO_4$ powder was synthesized via a citrate complex route [23] and the target was prepared by compressing the raw powder under a uni-axial pressure of 300 MPa and then sintered at 900°C in air for 3 hours. The prepared $CaWO_4$ and $CaMoO_4$ targets were white-yellow in color and XRD measurement showed that the target had a single phase which was consistent with reported value (*insets* of Fig. 3, JCPDS Cards 41-1431 ($CaWO_4$) and 29-0351 ($CaMoO_4$)). After removing organic contaminations with ultrasonic cleaner in acetone, the cleaned target was immersed into 60 ml ethanol, thereafter the target was irradiated by the Nd : YAG pulsed laser. The laser beam was focused on the target with a beam size of about 1 mm in diameter using a lens with a focal length of 50 mm. The depth of the target immersed into the de-ionized water was kept about 20 mm. Colloidal suspension of $CaWO_4$ and $CaMoO_4$ nanoparticles were obtained by laser ablation for 3 hours at room temperature.

2.2. Particle Size Distribution Analysis by Nanoparticle Tracking

The particle size distributions of the synthesized colloidal suspensions were statistically analyzed by nanoparticle tracking analysis method by HALO LM 10^{TM} system (Nano Sight, UK [22]) in Fig. 3. The class 1 laser device comprises a small Al metal housing (92 × 66 × 47 mm) containing a solid-state, single mode laser diode (< 20 mW, 655 nm) configured to launch a finely focused beam through the 500 μl *s*ample chamber. The chamber is

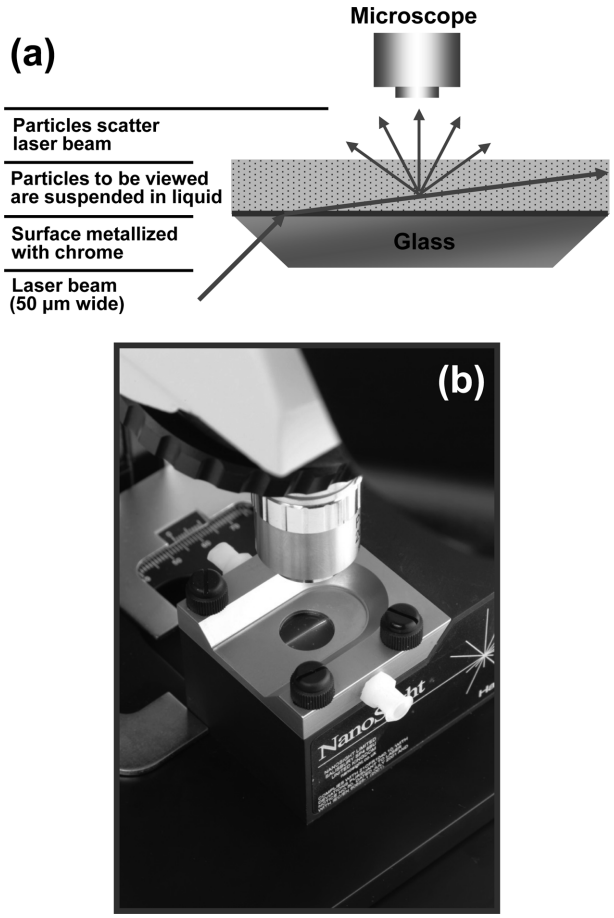

Fig. 2. (a) Schematic diagram for detecting nanoparticles in laser viewing module. A laser beam is fired into a suspension of nanoparticles in liquid. As the beam hits the particles, the light they scatter can be detected using a conventional microscope. (b) The HALO system consists of HALO LM10 viewing module and microscope [22].

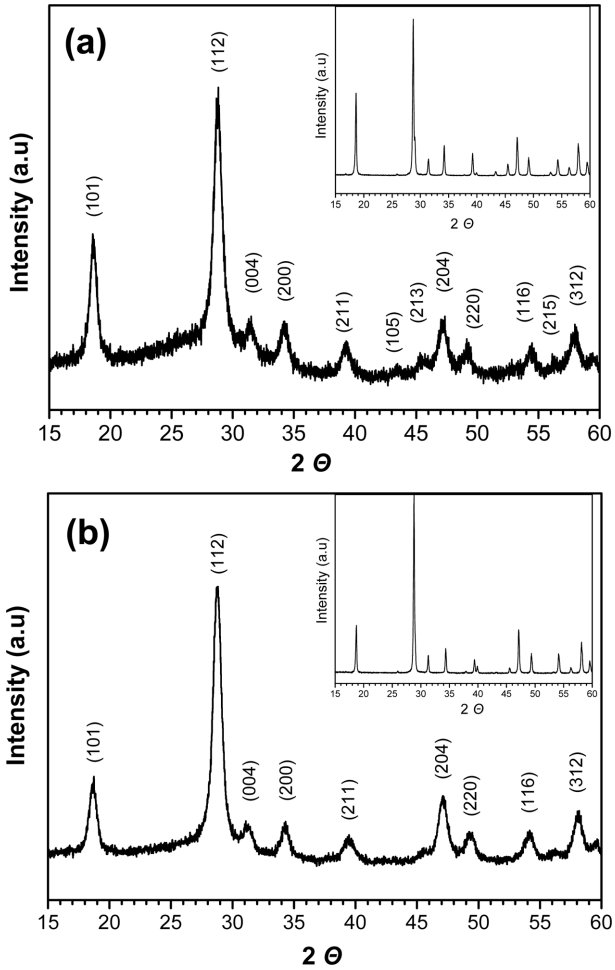

Fig. 3. X-ray diffraction patterns of (a) $CaWO_4$ and (b) $CaMoO_4$ nanoparticles collected from colloidal suspensions. The XRD patterns of the targets are shown as insets.

defined by an upper optical window mounted in a detachable stainless steel top-plate through which the sample is viewed down the microscope. The base of the chamber comprises a specially designed metallized optical flat above which the beam is caused to propagate in close proximity to the metal film. Particles in the liquid sample, and which pass through the beam path, are seen down the microscope as small points of light moving rapidly under Brownian motion. Sample is simply introduced into the chamber by syringe via the Luer fittings and allowed to equilibrate to unit temperature for a minute.

A more attractive alternative, given the ability of this nanoparticle tracking system to visualize deeply submicron particles in real time and in liquids, is to dynamically analyze the paths the particles take under Brownian motion over a suitable period to time (e.g. 10~20 seconds). Despite the rapidity with which particles move (in the sub-100 nm size range in particular), such motion can be readily tracked using conventional digital camcorder employed in. Supported on a mount of the microscope and operating at 20 frames per seconds, the camcorder is used to capture video clips of the particles as seen at a total magnification of 1000 when present in the 80 μm diameter laser beam within the device. It should be noted that, however, the particles are not being imaged. The particles act as point scatters whose dimensions are far below the Rayleigh or Abbé limit, only above which can structural information and shape be resolved.

2.3. Phase Analysis and Optical Characterizations

Surface morphology of the ablated $CaWO_4$ and $CaMoO_4$ ceramic targets was observed with a scanning electron microscope (SEM, JEOL, JSM 5900 LV, Japan). The suspensions were dropped on a carbon-coated copper grid for transmission electron microscope (TEM, JEOL, JEM-2010, 200 kV, Japan) observation. Precipitates of

the products were obtained by repeated centrifuging at 25,000 rpm for 30 min using an ultracentrifuge (Supra 25K, Hanil Sci. & Ind. Co., Korea). The X-ray diffraction (XRD, CuK_{α}, 40 kV, 30 mA, Rigaku, Japan) measurements were performed for the centrifuged precipitates. The optical absorbance of the $CaWO_4$ and $CaMoO_4$ nanoparticle-dispersed suspensions were evaluated using UV-Vis spectrophotometer (Optizen 2120 UV, Mecasys, Korea) and the photoluminescence (PL) spectrum was recorded using a luminescence spectrometer (PerkinElmer LS45, USA) at room temperature.

3. Results and Discussion

3.1. Formation of Colloidal Nanoparticles and Laser Ablation Mechanism

Fig. 3 depicts XRD spectra of the (a) $CaWO_4$ and (b) $CaMoO_4$ nanoparticles collected from colloidal suspensions prepared by pulsed laser ablation in ethanol. The Bragg reflection peaks of the nanoparticles collected from the colloidal suspension corresponded with the scheelite structured $CaWO_4$ and powellite structure of $CaMoO_4$ without any peaks assigned to either Ca, CaO, $CaCO_3$, W, Mo, WO_3 or MoO_3 phases. The broad reflection peaks in Fig. 3 indicate the formation of very small nanoparticles.

The particle morphology, particle size and crystallinity were more directly investigated using a TEM as shown in Fig. 4. It is found that most of the nanoparticles are spherical and homogeneous with diameter of 5~50 nm. Selected area electron diffraction (SAED) patterns revealed that the $CaWO_4$ and $CaMoO_4$ nanoparticles were crystallized with bright polycrystalline diffraction rings (*insets* of Fig. 4). The lattice spacing obtained form the diffraction rings agreed well with those of the scheelite $CaWO_4$ and powellite $CaMoO_4$.

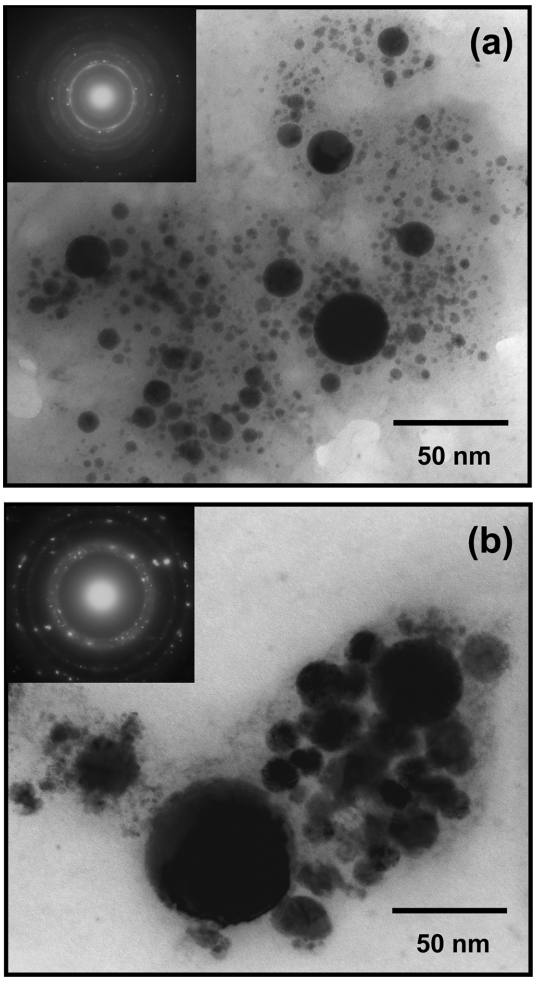

Fig. 4. TEM images of (a) $CaWO_4$ and (b) $CaMoO_4$ nanoparticles prepared by pulsed laser ablation in ethanol. Insets depict the electron diffraction patterns.

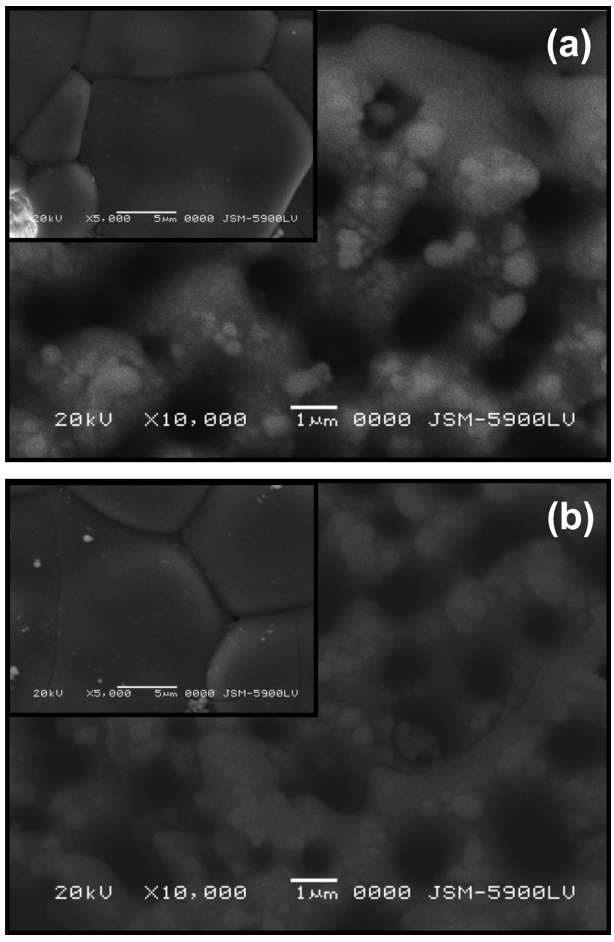

Fig. 5. Typical surface micrographs of the (a) $CaWO_4$ and (b) $CaMoO_4$ ceramic targets after laser ablation. And, typical SEM micrographs of target surface before laser irradiation are shown in *insets* for investigating the change of surface morphology by laser ablation.

Fig. 5 presents typical surface topographies of the $CaWO_4$ and $CaMoO_4$ targets after laser irradiation and before (as insets) in order to analyze the surface morphology change induced by laser irradiation. The laser ablation of solids in liquid medium occurs when a high-power laser beam is focused at the submerged target surface for an appropriate time, and leads to the ejection of particles to the liquid where they are condensed and cooled. Molecular dynamics simulations [24-26] have proposed two different mechanism of particle removal during ablation: below a given fluence threshold, there is desorption that is characterized by events in which primary individual atom desorb. Above this threshold, the ejected plume contains a substantial fraction of large molecular clusters.

The formation of the $CaWO_4$ and $CaMoO_4$ nanoparticles under laser irradiation can be thought to be due to a strong interaction of the ejected plume with surrounding ethanol molecules. Both microscopic observation of the nanoparticles in Fig. 4 and the surface aspects of the target after irradiation in Fig. 5 indicate that the fluence threshold was surpassed. Indeed, a thin layer of target is heated well above its melting temperature during the laser pulse. The adjacent ethanol molecules are heated to almost the same temperature owing to heat transfer form the interface. Taking into account the heat diffusion coefficient in ethanol ($a = 10^{-3}$ cm^2/s), the diffusion time approximately equal to duration of the laser pulse ($t_p = 8$ ns), and the thickness of the heated liquid layer h can be estimated approximately to $\sim (at_p)^{1/2} = 0.03$ μm. Therefore, after just 5 pulses at the same focal point, i.e. after only 0.5 s, the estimated ethanol bubble has a radius about 0.15 μm. This radius is greater much than the particle size verified in the experiments. Therefore, the condensation of the $CaWO_4$ and $CaMoO_4$ may occur in the ethanol vapor medium.

This means that the ablation process in liquid is not far different from those occurring at normal atmosphere, with just one important difference, where the pressure inside the bubbles should be very high. The interaction of the plume and the ethanol vapor leads to condensation and fast agglomeration to clusters. Observing the surface damage in Fig. 5, it can be considered that the ablation mechanism is photo-ablation of particles being formed from a superheated liquid. In the case of ablation due to desorption of small clusters, i.e., below the fluence threshold, the surface should be more flat and less rough [24-26]. It seems that this is not the case here. Therefore, the particles observed in TEM, e.g. diameters of 5~50 nm are considered to result from condensed clusters and recast droplets from the targets.

3.2. Size Distribution Analysis of Nanocolloidal Particles by Laser Scattering

The video images of the $CaWO_4$ and $CaMoO_4$ colloidal particles' movement under Brownian motion were analyzed using a single particle tracking program (Halo™ 2.2 image analysis software). In the system described here, a video can be either captured directly from the camera through the program or imported as a separate file. Fig. 6 shows the captured image of (a) $CaWO_4$ and (b) $CaMoO_4$ particles scattered by laser beam. The first frame of the 8 bit video sequence was deleted in terms of image smoothing, background subtraction, setting of thresholds, removal of blurring etc. to allow particles of interest to be tracked without interference from stray flare or diffraction patterns which can occasionally occur with non-optimum sample types.

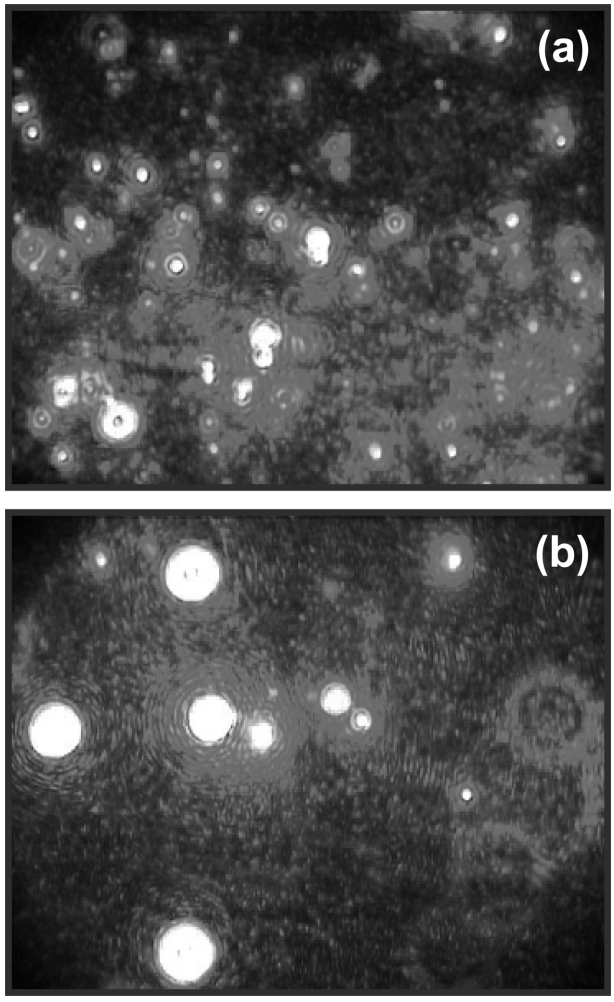

Fig. 6. Captured images of (a) $CaWO_4$ and (b) $CaMoO_4$ nanoparticles scattered by laser beam.

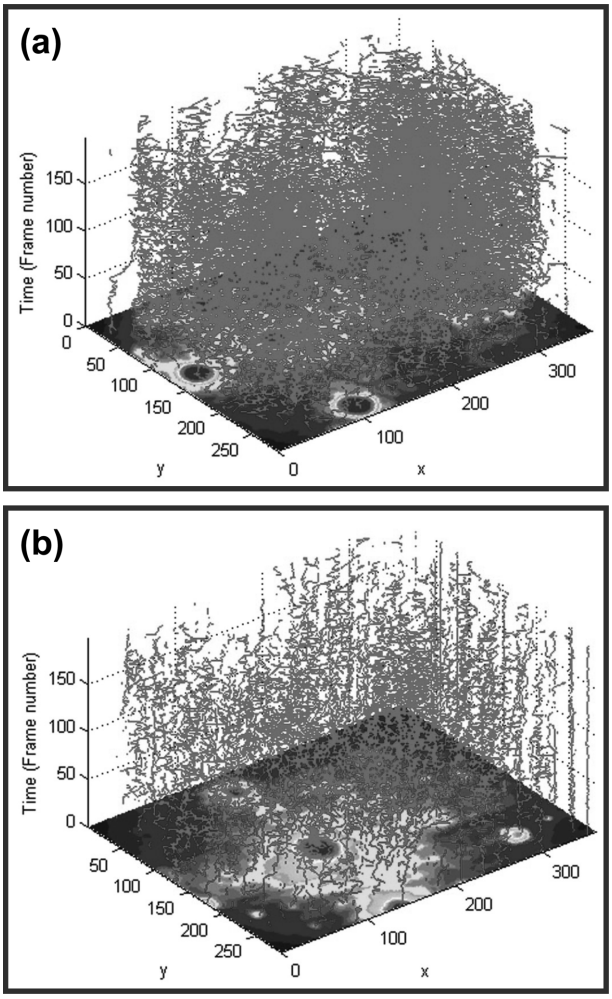

Fig. 7. Trajectories of (a) $CaWO_4$ and (b) $CaMoO_4$ colloidal nanoparicles whose life time are sufficiently long to ensure statistically accurate results.

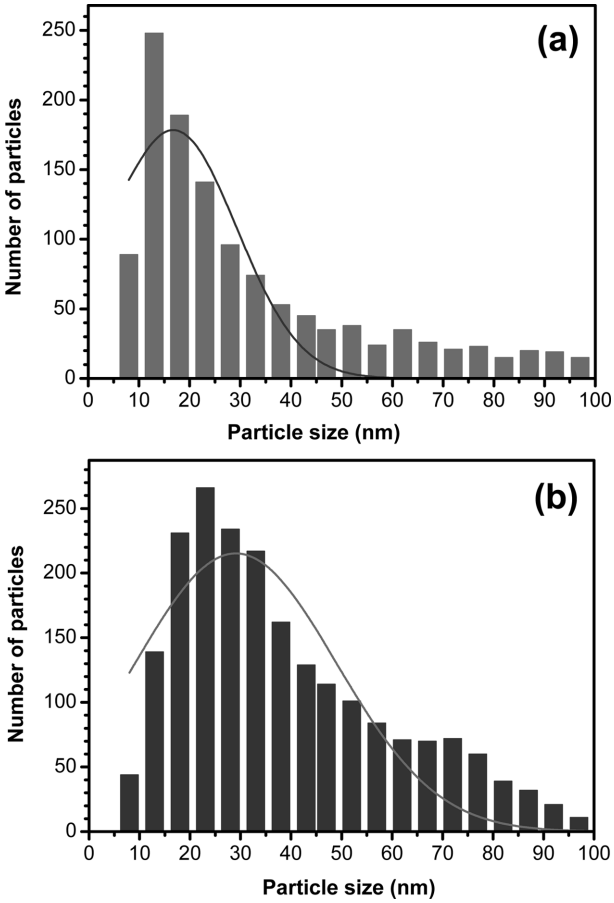

Fig. 8. Particle size distributions of (a) $CaWO_4$ and (b) $CaMoO_4$ nanocolloidal suspensions calculated by Brownian motion. These results came from measurements of individual particles, avoiding the averaging assumptions inherent from photon correlation spectroscopy.

Having selected suitable image adjustment setting, the remainder of the video was similarly treated allowing particles to be identified and located on a frame-by-frame basis. Through use of specific selection criteria, movement of individual particles was followed through the video sequence and the root-mean squared displacement determined for each particle for as long as it is visible.

We selected trajectories of colloidal nanoparticles whose lifetimes are sufficiently long to ensure statistically accurate results, as shown in Fig. 7(a~b), ignoring those which are so short (e.g. below 5 or 10 frames) that the estimation of diffusion coefficient is statistically inaccurate. Similarily the occurrence of trajectory cross-over could be accounted for thereby minimizing error. From these values, the diffusion coefficient (D_t) and hence sphere-equivalent, hydrodynamic radius (r_h) of the $CaWO_4$ and $CaMoO_4$ colloidal nanoparticles could be determined using the Stokes-Einstein equation [27]:

$$D_t = \frac{K_B T}{6\pi\eta r_h} \quad (1)$$

where K_B is Boltzmann's constant, T is temperature and η is viscosity of liquid. Given that each and every visible particle is separately tracked, it is possible to generate particle size distributions profiles that reflect the actual number of particles thus seen and which is a significnat advance on those distributions that are obtained by other dynamic light scattering techniques such as photon correlation spectroscopy (PCS) in which a large ensemble of particles are collectively analyzed [28].

Particle size distributions of the $CaWO_4$ and $CaMoO_4$ colloidal nanoparticles obtained from the nanoparticle tracking system are shown in Fig. 8. Gaussian fittings were applied to the size distribution (the solid line in Fig. 8). From the Gaussian distributions, it is found that the mean nanoparticle size of $CaWO_4$ and $CaMoO_4$ colloidal nanoparticles were 16 nm and 30 nm, with the standard deviations of 2.1 and 5.2 nm, respectively. The

$CaMoO_4$ naoparticles (Fig. 8(b)) presented a large diameter distribution between 5 and 100 nm, a peak centered at 20~25 nm, and 57 % of tracked particles had more than 30 nm diameter. On the other hand, the $CaWO_4$ nanoparticles (Fig. 8(a)) presented better diameter convergence than $CaMoO_4$, since neraly 62 % of the tracked nanoparticles were between 5 and 30 nm and only 20 % were greater than 50 nm. These results are in good agreement with the particle size analysis given by TEM. We note that there are no droplets detected of diameter bigger than 100 nm.

3.3. Optical Properties of the $CaWO_4$ and $CaMoO_4$ Colloidal Suspensions

Optical absorption spectra of the $CaWO_4$ and $CaMoO_4$ nanoparticles-dispersed colloids are presented in *insets* of Fig. 9(a~b). The sharp spectra with high absorbance in the UV region indicate formation of stable colloidal suspensions. The absorption spectra showed a typical absorption edge near 250 nm, which is blue-shifted about 50 and 70 nm than the reported value (near 300 nm in $CaWO_4$ [29] and 340 nm in $CaMoO_4$ [30]). The $CaWO_4$ and $CaMoO_4$ have direct band-gaps of 4.09 and 3.41 eV in the Γ direction, respectively, calculated by using the linearized-augmented-plane-wave technique [31] and fundamental absorption of the $CaWO_4$ and $CaMoO_4$ is attributed to a charge-transfer transition in which an oxygen 2p electron goes into one of the empty molybdenum 4d or tungsten 5d orbitals [31]. The optical band-gap energies, E_{gap}, for the $CaWO_4$ and $CaMoO_4$ nanoparticles were determined from the most sharply increasing absorption region according to Tauc and Menth's law [32]. The plot of $(\alpha h\nu)^2$ versus photon energy ($h\nu$) are displayed in Fig. 9(a~b). In the high energy region of the absorption edge, $(\alpha h\nu)^2$ varied linearly with $h\nu$

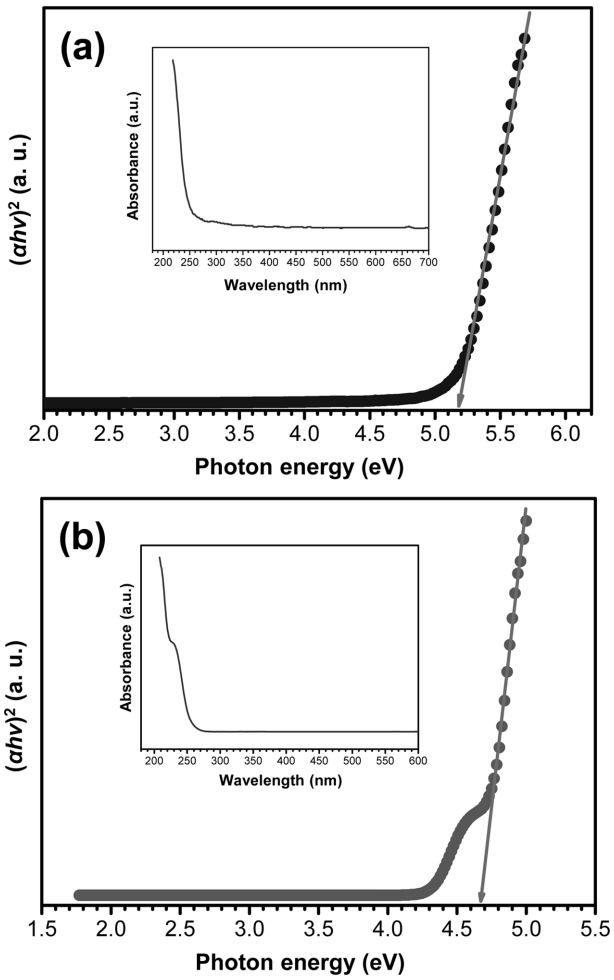

Fig. 9. The plots of $(\alpha h\nu)^2$ versus photon energy ($h\nu$) in case of (a) $CaWO_4$ and (b) $CaMoO_4$ suspensions prepared by pulsed laser ablation in ethanol. Insets represent optical absorption spectra of the nanocolloidal suspensions.

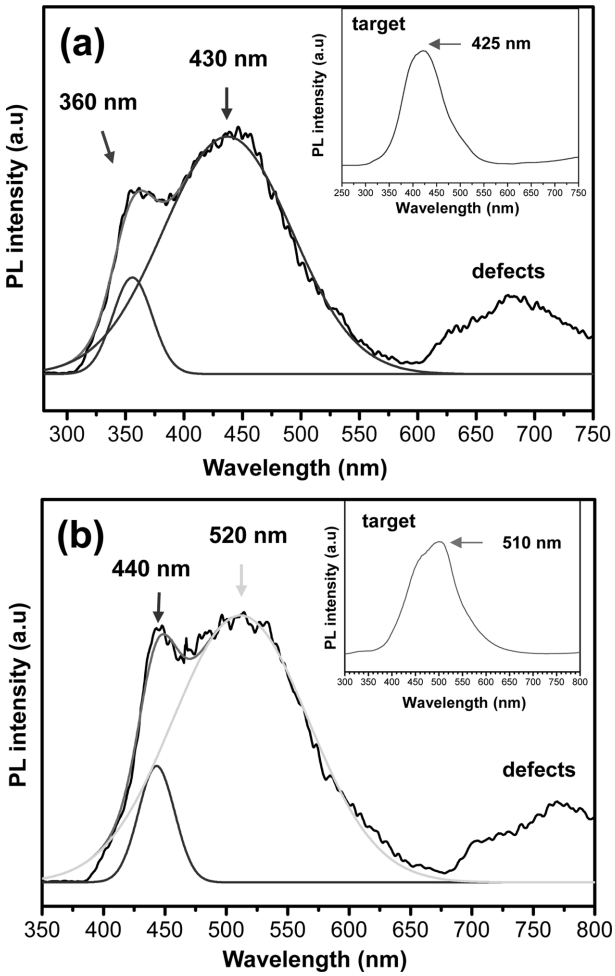

Fig. 10. Room-temperature PL spectra of the (a) $CaWO_4$ and (b) $CaMoO_4$ nanocolloidal suspensions. Insets show the PL spectra of the bulk targets for comparison with the prepared nanocolloidal suspensions.

and the straight line behavior in the high energy region was taken as prime evidence for the direct band-gap. The estimated optical band-gaps were 5.2 ($CaWO_4$) and 4.7 eV ($CaMoO_4$), which is an increased value about 1.1 and 1.3 eV compared to the reported theoretical band-gap energy [31].

Photoluminescence (PL) spectra obtained from the $CaWO_4$ and $CaMoO_4$ colloidal suspensions are shown in Fig. 10(a~b). The PL spectra were obtained at an excitation of 240 nm. The decomposition of the PL bands into individual Gaussian components resulted in two Gaussian curves to achieve good agreement with the experimental data, which are given in Fig. 10(a~b). Most studies on the PL of $CaWO_4$ and $CaMoO_4$ crystals have reported blue and green emission near 420 and 530 nm, respectively, for excitations between 240 and 280 nm [33-35] at room temperature. Consisted with the widened optical band-gap estimated from the Tauc plots in Fig. 9(a~b), the colloidal suspensions exhibited blue-shifted emission peaks near 360 and 440 nm besides inherent main PL peaks. For comparison, PL spectra of the bulk $CaWO_4$ and $CaMoO_4$ targets are shown in *insets* of Fig. 10(a~b). The existence of the blue-shifted PL spectra in the colloidal suspensions is thought to be originated mainly from the very small nanocrystalline constituents as investigated in TEM and nanoparticle tracking analysis.

The band-gap widening phenomena and blue-shifts in the absorption edges and PL emissions can be attributed mainly to quantum-size effect induced by the very small size of the $CaWO_4$ and $CaMoO_4$ nanoparticles prepared by pulsed laser ablation in ethanol. In the colloidal suspensions, there exist very small nanocrystals, grain boundaries and imperfections as shown in TEM and nanoparticle tracking analysis, which lead to larger free carrier concentrations and the existence of potential barriers at the boundaries. Therefore, an electric field is formed and this brings about an increase of the band-gap. The quantum-size effect results in a dramatic increase in the band-gap if the crystallite dimensions become very small. For our $CaWO_4$ and $CaMoO_4$ colloidal suspension, there are many nanocrystals with the size smaller than of 20 nm in the $CaWO_4$ and $CaMoO_4$ particles, which have influence on the value of the band-gap. In addition, a weak red or infrared emission bands were observed from 750 to 850 nm. The additional emission bands can be interpreted by the existence of Frenkel defects structure (oxygen ion shifted to the inter-site position with simultaneous creation of vacancy) in the surface layers of nanocrystallites [36] similar to what is observed in following references [37].

4. Summary

This work demonstrated the formation of $CaWO_4$ and $CaMoO_4$ nanocolloidal suspensions using pulsed laser ablation in ethanol without any surfactant. The obtained $CaWO_4$ and $CaMoO_4$ nanoparticles had spherical and highly-dispersed morphology. The mechanism of laser ablation was explained as photo-ablation where particles were generated by rapid solidification from the melt. Particle tracking analysis by optical microscopy combined with image analysis allowed for a fast determination of particle size distribution function in the prepared nanocolloidal suspensions. From the determined particle size distribution functions, it was found that the mean nanoparticle size of the prepared $CaWO_4$ and $CaMoO_4$ colloidal nanoparticles were 16 nm and 30 nm, with the standard deviations of 2.1 and 5.2 nm, respectively, which are in good agreement with the particle size analysis given by TEM. The absorption spectra and PL emissions of the $CaWO_4$ and $CaMoO_4$ colloidal suspensions showed highly blue-shifted values. The estimated optical band-gap values of the $CaWO_4$ and $CaMoO_4$ nanoparticles was 5.2 and 4.7 eV, which was a widened value about 1.1 and 1.3 eV, than that of reported theoretical from bulk crystals, respectively. These band-gap widening and blue-shifts in absorption edge and PL emission could be ascribed to the quantum-size effect caused by the very small size of the prepared colloidal suspensions.

Acknowledgment

This research was supported by Basic Science Research Program through the National Research Foundation of Korea (NRF) funded by the Ministry of Education, Science and Technology (2012R1A1A2039956).

References

[1] A. Fojtik, M. Giersig and A. Henglein, “Formation of nanometer-size silicon particles in a laser induced plasma in SiH_4”, Ber. Bunsenges. Phys. Chem. 97 (1993) 1493.
[2] J. Heddersen, G. Chumanov and T.M. Cotton, “Laser ablation of metals: A new method for preparing SERS active colloids”, Appl. Spectrosc. 47 (1993) 1959.
[3] A.V. Simakin, V.V. Voronov, G.A. Shafeev, R. Brayner and F.B. Verduraz, “Nanodisks of Au and Ag produced by laser ablation in liquid environment”, Chem. Phys. Lett. 348 (2001) 182.
[4] R.A. Ganeev, M. Baba, A.I. Ryasnyansky, M. Suzuki

and H. Kuroda, "Characterization of optical and nonlinear optical properties of silver nanoparticles prepared by laser ablation in various liquids", Opt. Commun. 240 (2004) 437.
[5] G.A. Shafeev, E. Freysz and F.B. Verduraz, "Nanoparticles produced by laser ablation of solids in liquid environment", Appl. Phys. A 78 (2004) 307.
[6] A. Iwabuchi, C.-K. Choo and K. Tanaka, "Titania nanoparticles prepared with pulsed laser ablation of rutile single crystals in water", J. Phys. Chem. B 108 (2004) 10863.
[7] K.V. Anikin, N.N. Melnik, A.V. Simakin, G.A. Shafeev, V.V. Voronov and A.G. Vitukhnovsky, "Formation of ZnSe and CdS quantum dots via laser ablation in liquids", Chem. Phys. Lett. 366 (2002) 357.
[8] R.A. Ganeev, M. Bara, A.I. Ryasnyansky, M. Suzuki and H. Kuroda, "Nonlinear refraction in CS", Appl. Phys. B 80 (2005) 595.
[9] T. Tsuji, T. Hamagami, T. Kawamura, J. Yamaki and M. Tsuji, "Laser ablation of cobalt and cobalt oxides in liquids: influence of solvent on composition of prepared nanoparticles", Appl. Surf. Sci. 243 (2005) 214.
[10] H. Lange, "Comparative test of methods to determine particle size and particle size distribution in the submicron range", Part. Part. Syst. Charact. 12 (1995) 148.
[11] S. Lee, S.P. Rao, M.H. Moon and J.C. Giddings, "Determination of mean diameter and particle size distribution of acrylate latex using flow field-flow fractionation, photon correlation spectroscopy, and electron microscopy", Anal. Chem. 68 (1996) 1545.
[12] O. Elizalde, G.P. Leal and J.R. Leiza, "Particle size distribution measurements of polymeric dispersions: A comparative study", Part. Part. Syst. Charact. 17 (2000) 236.
[13] T. Provder, "Characterization of compositional heterogeneity in copolymers and coatings systems by GPC/FTIR", Prog. Org. Coat. 32 (1997) 143.
[14] W. Schaertl and H. Sillescu, "Dynamics of colloidal hard spheres in thin aqueous suspension layers-particle tracking by digital image processing and brownian dynamics computer simulations", J. Colloid Interface Sci. 155 (1993) 313.
[15] J.C. Crocker and D.G. Grier, "Methods of digital video microscopy for colloidal studies", J. Colloid Interface Sci. 179 (1996) 298.
[16] B. Carr, T. Diaper and E. Barrett, Royal Society of Chemistry, Particulate System Analysis 2005, Stratford-upon-Avon, UK. p. 1.
[17] S.H. Yu, B. Liu, M.S. Mo, J.H. Huang, X.M. Liu and Y.T. Qian, "General synthesis of single-crystal tungstate nanorods/nanowires: A facile, low-temperature solution approach", Adv. Funct. Mater. 13 (2003) 639.
[18] R. Grasser, E. Pitt, A. Scharmann and G. Zimmerer, "Optical properties of $CaWO_4$ and $CaMoO_4$ crystals in the 4 to 25 eV region", Phys. Status Solidi B 69 (1975) 359.
[19] J.H. Ryu, J.-W. Yoon, C.S. Lim, W.-C. Oh and K.B. Shim, "Microwave-assisted synthesis of nanocrystalline MWO_4 (M: Ca, Ni) via water-based citrate complex precursor", Ceramics International 31 (2005) 883.
[20] A. Sen and P. Pramanik, "A chemical synthetic route for the preparation of fine-grained metal tungstate powders (M = Ca, Co, Ni, Cu, Zn)", J. Eur. Ceram. Soc. 21 (2001) 745.
[21] W. Sleight, "Accurate cell dimensions for ABO_4 molybdates and tungstates", Acta Crystallogr. B 28 (1972) 2899.
[22] W.S. Cho, M. Yashima, M. Kakihana, A. Kudo, T. Sakata and M. Yoshimura, "Active electrochemical dissolution of molybdenum and application for room-temperature synthesis of crystallized luminescent calcium molybdate film", J. Am. Ceram. Soc. 80 (1997) 765.
[23] J.H. Ryu, J.-W. Yoon, C.S. Lim, W.-C. Oh and K.B. Shim, "Microwave-assisted synthesis of $CaMoO_4$ nano-powders by a citrate complex method and its photoluminescence property", J. Alloys and Compd. 390 (2005) 245.
[24] L.V. Zhigilei, P.B.S. Kodali and B.J. Garrison, "A microscopic view of laser ablation", J. Phys. Chem. B 102 (1998) 2845.
[25] A.A. Oraevsky and S.L. Jacques, "Mechanism of laser ablation for aqueous media irradiated under confined-stress conditions", J. Appl. Phys. 78(2) (1995) 1281.
[26] L.V. Zhigilei, "Dynamics of the plume formation and parameters of the ejected clusters in short-pulse laser ablation", Appl. Phys. A 76 (2003) 339.
[27] T. Tixier, M.H. Butler and E.M. Terentjev, "Spontaneous size selection in cholesteric and nematic emulsions", Langmuir 22 (2006) 2365.
[28] R. Pecora (Ed.), Dynamic light scattering, application of photon correlation spectroscopy, Plenum Press, New York (1985).
[29] R. Zhai, H. Wang, H. Yan and M. Yoshimura, "Preparation of crystalline $CaWO_4$ thin films by chemical bath deposition", J. Cryst. Growth 289 (2006) 647.
[30] L.B. Barbosa, D.R. Ardila, C. Cusatis and J.P. Andreeta, "Growth and characterization of crack-free scheelite calcium molybdate single crystal fiber", J. Cryst. Growth 235 (2002) 327.
[31] Y. Zhang, N.A.W. Holzwarth and R.T. Williams, "Electronic band structures of the scheelite materials $CaMoO_4$, $CaWO_4$, $PbMoO_4$, and $PbWO_4$", Phys. Rev. B 57(20) (1998) 12738.
[32] J. Tauc and A. Menth, "Magnetic susceptibility of amorphous semiconductors", J. Non-Cryst. Solids 8/9 (1972) 569.
[33] W. Van Loo, "Luminescence of lead molybdate and lead tungstate. I. Experimental", Phys. Status Solidi A 27 (1975) 565.
[34] B.K. Chandrasekhar and W.B. White, "Luminescence of single crystal $CaMoO_4$", Mat. Res. Bull. 25 (1990) 1513.
[35] D. Spassky, S. Ivanov, I. Kitaeva, V. Kolobanov, V. Mikhailin, L. Ivleva and I. Voronina, "Optical and luminescent properties of a series of molybdate single crystals of scheelite crystal structure", Phys. Status Solidi C 2 (2005) 65.
[36] V.B. Mikhailik, H. Kraus, D. Wahl and M.S. Mykhaylyk, "Studies of electronic excitations in $MgMoO_4$, $CaMoO_4$ and $CdMoO_4$ crystals using VUV synchrotron radiation", Phys. Status Solidi B 242 (2005) R17.
[37] R. Grasser, A. Scharmann and K.-R. Strack, "On the intrinsic nature of the blue luminescence in $CaWO_4$", J. Lumin. 27 (1982) 263.